doi: 10.1111/j.1460-2695.2006.01019.x

Measurement of crack bridging stresses in environment-assisted cracking of duplex stainless by synchrotron diffraction

T. J. MARROW[1], A. STEUWER[2], F. MOHAMMED[1], D. ENGELBERG[1] and M. SARWAR[3]

[1]*School of Materials, University of Manchester, UK,* [2]*FaME38 (Facility for Materials Engineering), ILL-ESRF, Grenoble, France,* [3]*NMD. PINSTECH, P. O. Nilore, Islamabad, Pakistan*

Received in final form 27 January 2006

ABSTRACT Crack propagation studies have been conducted in age-hardened Zeron 100 duplex stainless steel, which in the 475 °C embrittled condition exhibits environment-assisted cracking under cathodic conditions in aqueous 3.5% NaCl solution. Values of the threshold stress intensity for environment-assisted cracking, K_{1SCC}, measured by crack arrest, show *R*-curve behaviour. Diffraction experiments on the high-energy beamline ID15A at the European Synchrotron Radiation Facility (ESRF) were performed to measure the crystal lattice strains in ferrite and austenite in wedge open loaded (WOL) stress corrosion specimens. The observations demonstrate that significant crack bridging stresses develop in the wake of the crack. This is due to branching of the environment-assisted crack. Simple bridging models for the effect of the measured stresses are in agreement with the observed *R*-curve behaviour.

Keywords crack bridging; duplex stainless steel; environment-assisted cracking; synchrotron X-ray diffraction.

NOMENCLATURE

d_{hkl}	Interplanar spacing of the (hkl) crystal lattice planes
K_{1SCC}	Measured threshold stress intensity factor for environment-assisted cracking
K_0	Intrinsic threshold stress intensity factor for environment-assisted cracking of a non-bridged crack
K_{max}	Maximum stress intensity factor
R-curve	Rising crack propagation resistance with crack extension
SCE	Electrochemical potential (mV) relative to Standard Calomel Electrode
WOL	Wedge open loaded
X	Co-ordinate perpendicular to the fatigue crack plane and perpendicular to the crack propagation direction
Y	Co-ordinate perpendicular to the fatigue crack plane and parallel to the crack propagation direction
Z	Co-ordinate in the fatigue crack plane and perpendicular to the crack propagation direction
σ_{sh}	Average shielding stress
∂a	Crack extension
2θ	Diffraction angle

INTRODUCTION

The high strength, toughness and corrosion resistance of ferrite-matrix duplex stainless steels are required in the offshore oil and gas industry. Environment-assisted cracking failures in duplex stainless steels are uncommon, but are particularly expensive when offshore components require repair or recovery from the seabed. Failures have been reported to occur under cathodic protection, Ref. [1] for example. It is therefore necessary to identify microstructures that are susceptible to brittle fracture and environment-assisted crack propagation and which may, particularly in the anisotropic microstructures of large forgings, permit easy and fast crack growth. This requires

Correspondence: J. Marrow. E-mail: james.marrow@manchester.ac.uk

an understanding of the interaction between a propagating environment-assisted crack and the microstructure.

The experiment reported in this paper is the first attempt to investigate the magnitude of bridging stresses associated with environment-assisted cracking of a bulk sample by synchrotron X-ray diffraction methods. Conventional diffraction methods for elastic strain measurement on laboratory X-ray sources are limited to surface observations. Strain mapping in bulk samples can be achieved by neutron diffraction methods[2] but usually at low spatial resolution of ~1 mm. With the high brilliance and photon energies of several tens and hundreds of keV at sources such as the European Synchrotron Radiation Facility (ESRF), lattice strains can be measured within the bulk with a spatial resolution of the order of a few tens of micrometers.[2–5] The short counting times (typically of the order of seconds per point) open up the possibility of measuring the evolution of the internal stress state in cracked samples in situ, as a function of external parameters such as temperature and applied stress. This offers a unique insight to damage development.

EXPERIMENTAL METHOD AND RESULTS

Crack propagation in duplex stainless steel

Crack propagation studies have been conducted in age-hardened Zeron 100 duplex stainless steel, which in the embrittled condition exhibits environment-assisted cracking under cathodic conditions.[6,7] Crack propagation occurs by hydrogen-assisted cleavage of the ferrite matrix and ductile tearing of the austenite. The microstructure in this condition provides a model system, suitable for the study of crack bridging mechanisms. Fatigue precracked wedge open loaded (WOL) specimens of Zeron 100, age-hardened at 475 °C for 100 h to cause embrittlement,[8] were bolt loaded and immersed in aqueous 3.5% NaCl solution at −900 mV_{SCE} for 14 d.[9] Crack propagation and subsequent arrest, i.e no detectable crack growth by optical examination, was observed. The load at crack arrest was taken as the applied load that was required to achieve the final crack mouth opening displacement. This was measured after crack arrest while the specimen was bolt loaded, followed by unloading (removal of the bolt) and then reloading the specimen using a tensile test machine with clip gauge monitoring. The unloaded specimen was then heat tinted at 450 °C for 30 min before breaking open to reveal the crack length. The stress intensity factor at arrest was calculated using the load at crack arrest and the heat-tinted crack length. Data from specimens which did not show a straight crack front (within the acceptance criteria of ASTM standard[10]) were discarded. The threshold stress intensity for environment-assisted cracking, K_{1SCC}, was considered to be equivalent to the value of stress intensity factor at crack arrest. The data were scattered but exhibited *R*-curve behaviour (Fig. 1),[9] i.e. rising crack propagation resistance with crack extension.

Metallographic observations (Fig. 2a) showed that crack bridging occurred on two length scales. Small-scale bridging ligaments were observed in a crack tip process zone that comprised cleaved ferrite bridged by ductile austenite (Fig. 2b and c). This zone was up to 5 mm long and spanned the width of the crack. Longer narrow

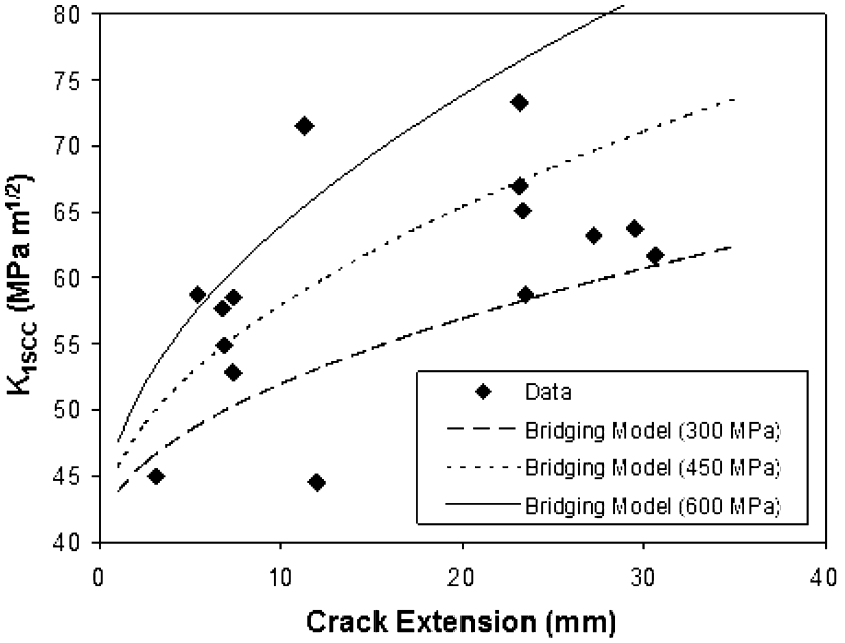

Fig. 1 Relationship between crack extension and stress intensity factor at arrest (K_{1SCC}) for stress corrosion cracking in age-hardened duplex stainless steel at −900 mV_{SCE} in aqueous 3.5 wt% NaCl. The influence of average crack bridging stresses between 300 MPa and 600 MPa on K_{1SCC} for a simple bridging model with an intrinsic environment-assisted cracking threshold of 40 MPa $m^{\frac{1}{2}}$ is also shown.

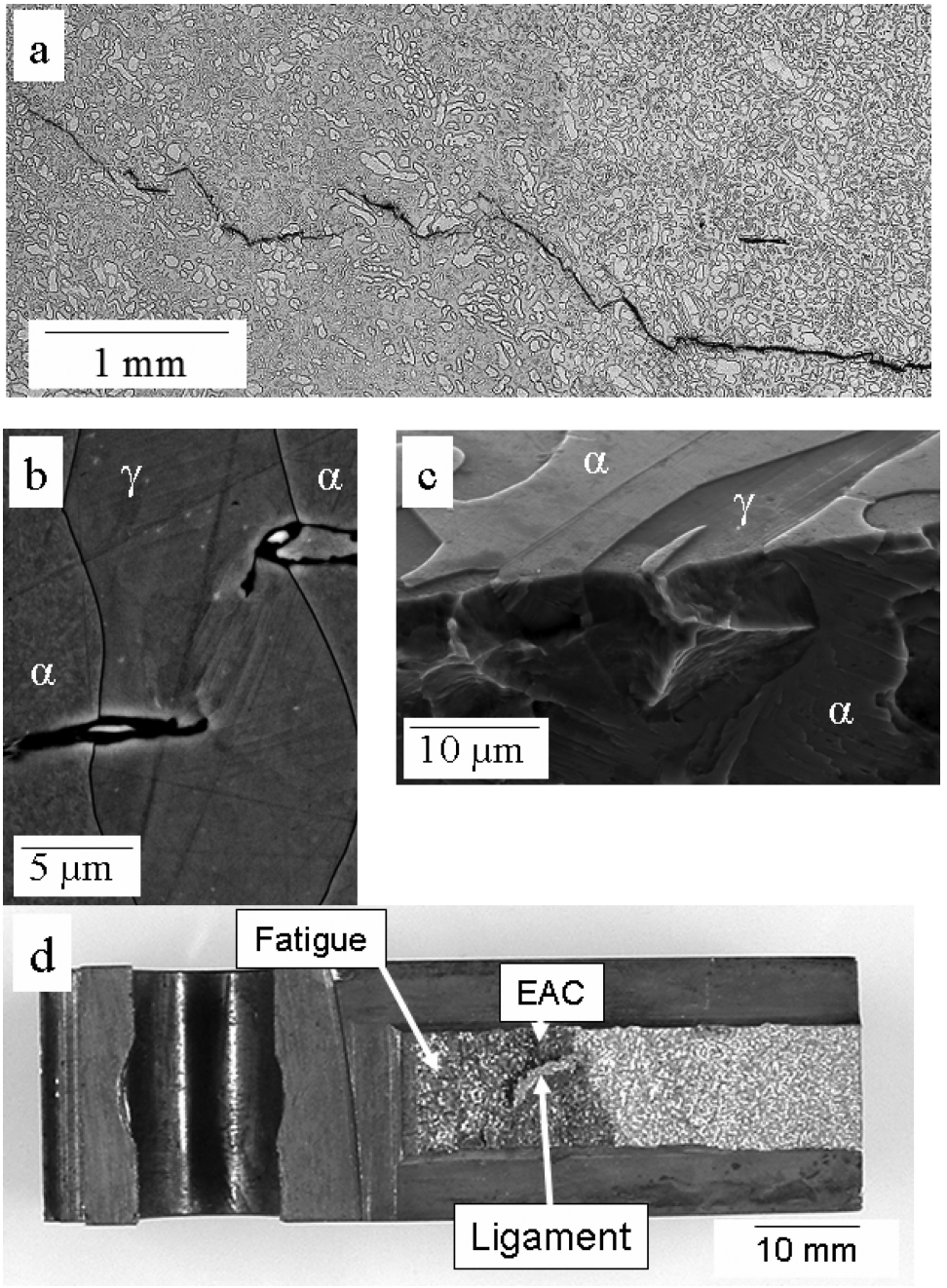

Fig. 2 Environment-assisted cracking in age-hardened Zeron 100 duplex stainless steel at −900 mV_{SCE} in 3.5 wt% NaCl: (a) crack bridging in the microstructure (crack growth from right to left), (b and c) ferrite (α) cleavage and austenite (γ) ductile fracture and (d) significant ligaments due to crack branching (The specimen was heat tinted after testing to reveal the crack surface).

ligaments, typically up to 5–10 mm in length, were the result of random branching and bifurcation of the crack plane (Fig. 2d). The effect of crack bridging on the specimen behaviour was shown by the *specimen stiffness error*. This described the difference between the measured and predicted stiffness[11] for the cracked WOL specimen, in terms of the ratio of the difference between the measured stiffness and the predicted stiffness to the predicted stiffness. Factors that decreased the measured specimen compliance increased the specimen stiffness error. The specimen stiffness error increased significantly with environment-assisted crack extension, to values of the order of 400% (Fig. 3). Observations from fatigue cracks gave specimen stiffness errors of less than 70% for all crack

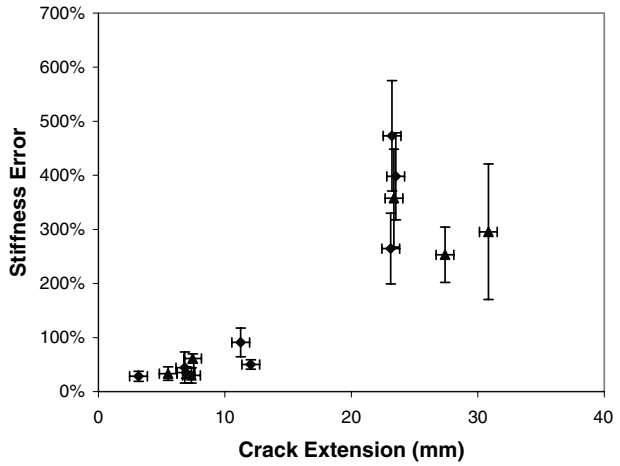

Fig. 3 The effect of crack extension on the specimen stiffness error (i.e. the difference between the measured specimen stiffness and the expected stiffness) for stress corrosion cracks in age-hardened Zeron 100 duplex stainless steel, tested at -900 mV_{SCE} in 3.5 wt% NaCl.

lengths.[9] The significant change in compliance for the environment-assisted cracks implied a significant degree of crack bridging, sufficient to cause crack tip shielding. Crack shielding would occur if the applied load was carried partly by the bridging ligaments and not fully transmitted to the crack tip.

A simple model for crack tip shielding due to crack bridging may be constructed which assumes that the critical stress intensity factor for environment-assisted crack propagation, (K_{1SCC}), is the intrinsic threshold stress intensity factor for the non-bridged crack (K_0) plus the shielding contribution due to an average stress (σ_{sh}) acting over the distance of crack extension (∂a). This is expressed in Eq. (1).[12] The increase in crack propagation resistance predicted by this shielding model is consistent with a shielding stress, σ_{sh}, of the order of 300–600 MPa, and an intrinsic K_0 of 40 MPa $m^{1/2}$ (Fig. 1). These values represent a shielding stress which is a significant fraction of the tensile yield strength (900 MPa) of the material, and the observed lower bound of the threshold stress intensity for environment-assisted cracking (Fig. 1).

$$K_{1SCC} = K_0 + \sqrt{\frac{2}{\pi}}\frac{\sigma_{sh}}{2}\sqrt{\partial a}. \quad (1)$$

The observations of increased specimen stiffness and rising environment-assisted cracking resistance are therefore consistent with crack bridging due to ligament formation in the crack wake. The synchrotron measurements of strain, which are the principle topic of this paper, were performed to confirm the magnitude and distribution of the crack bridging stresses.

Synchrotron mapping of strains

Specimen preparation and loading

The observations were performed using a bolt-loaded wedge opening load (WOL) specimen which had initially been side-grooved to give a central thickness of approximately 20 mm (full specimen thickness 25 mm, height 60 mm, width 80 mm). The side-grooving had previously been demonstrated to be necessary to give a planar crack.[9] The stress intensity factor correction for side-grooved WOL specimens is given in Ref. [11]. The specimen had been age-hardened at 475 °C for 100 h, and was then fatigue pre-cracked in air. The final maximum stress intensity factor, K_{max}, at the end of the fatigue pre-cracking was approximately 40 MPa $m^{1/2}$. Age hardening increased the Vicker's hardness from 270 to 330 HV_{30}. The specimen was tested at -900 mV_{SCE} in pH 7.5 NaCl solution (3.5 wt% in water) by bolt loading to an initial stress intensity factor of 60 MPa $m^{1/2}$ for 14 d.

The side groove on each side of the 25 mm thick specimen was initially 1 mm wide and 2.5 mm deep. This was widened and deepened after environment-assisted propagation of the crack to provide a 10 mm thick section for the strain-mapping experiment (Fig. 4). The 0.5% proof stress after age-hardening was approximately 900 MPa, thus the specimen thickness during the strain-mapping experiment would satisfy the approximate minimum thickness for plane strain conditions at an applied stress intensity factor of 60 MPa $m^{1/2}$.[10]

The specimen was stressed by bolt-loading during the strain-mapping experiment, and the applied load was confirmed by in situ measurement of the crack opening displacement using a clip gauge. The load-displacement behaviour of the cracked specimen had been calibrated after the widening of the side groove by loading to within 90% of the peak load to be applied during the strain-scanning experiment. Strain-mapping measurements were made with the specimen under zero load, then at various levels of load up to a stress intensity factor of 60 MPa $m^{1/2}$, and finally unloaded. All observations were made with the specimen in ambient air. There was no measurable difference between the crack opening displacement measurements before and after the experiment. Surface optical microscopy observations also showed that the crack did not propagate measurably during the experiment.

Strain-mapping and data analysis

The strain-mapping experiment was undertaken on beam line ID15A at the European Synchrotron Radiation Facility (ESRF) in energy dispersive mode with a fixed diffraction angle of 3.5°. The photon energy range selected was approximately 80–300 keV, which gave diffraction peaks in both ferrite and austenite. The sample was measured

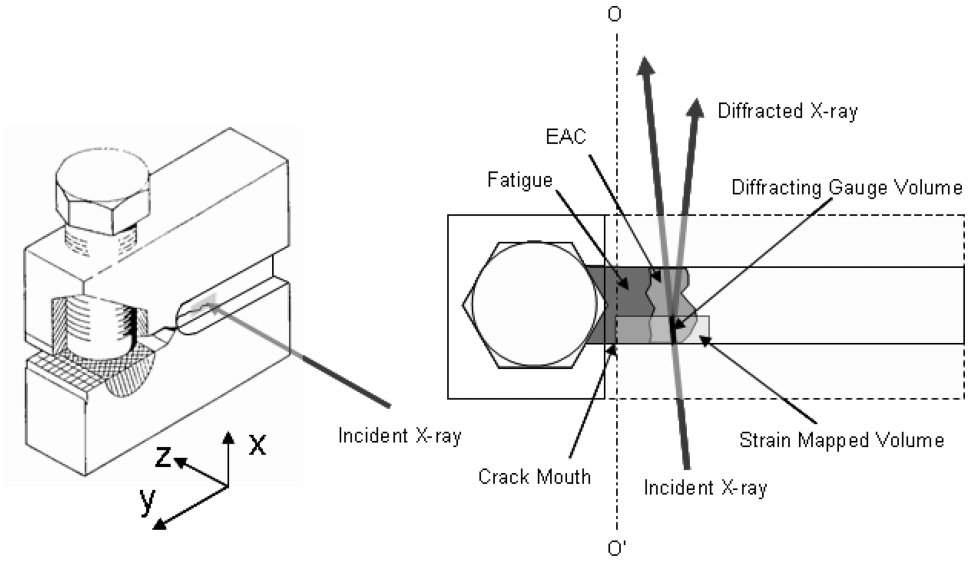

Fig. 4 Bolt loaded specimen with the location and orientation of the strain-mapped volume, containing the fatigue pre-crack and environment-assisted crack, defined by the diffracting gauge volume and scanned area.

in transmission mode with the direction of the scattering vector (i.e. the direction of strain measured) effectively perpendicular to the incident beam. The crack opening strains (mode I) were therefore measured. The region around the crack was mapped (in the X–Y plane) with a gauge volume defined by the 150 μm × 150 μm incident beam geometry at a diffraction angle, 2θ, of 3.5°. This diffraction angle gave the gauge volume, within which diffraction was detected, a depth of approximately 3 mm within the specimen in the Z direction (Fig. 4). The diffracting gauge volume was therefore approximately 0.07 mm^3, which was of the order of 500 grains (average grain size approximately 20 μm). The X–Y step size in the map was chosen to be either 0.1 mm or 0.2 mm, with a count time of 15 s. The sample was positioned such that the gauge volume was close to the edge of the sample (Fig. 4). The different step sizes had no measurable effect on the recorded data.

The diffraction setup and analysis methods are described in detail in Ref. [5], and the analysis method is summarized here briefly. The results were prepared using a Pawley refinement approach, using the software package GSAS (General Structure Analysis System, Los Alamos National Laboratory, CA, USA) in intensity-extraction mode. The collected spectra were transformed to an artificial, reciprocal scale, essentially equivalent to that of time-of-flight, and then stored using logarithmic rebinning in GSAS RALF (Rutherford Appleton Logarithmic Format). This allows the use of the asymmetric time-of-flight (TOF) neutron diffraction peak profiles (No. 3) in GSAS to determine the variation of the average crystal lattice d_{hkl}-spacing, with position of the gauge volume, in ferrite and austenite.

After the strain-mapping experiment, a rectangular section (approximately 15 mm × 10 mm × 5 mm) containing the strain-mapped volume was removed using a precision diamond saw. The rectangular section is indicated in Fig. 4. A series of metallographic sections in the X–Y plane were then obtained within the strain-mapped gauge volume at Z intervals of approximately 0.5 mm to determine the three-dimensional crack shape. Positioning agreement to within 0.25 mm, to correlate the strain-mapping measurements and the metallography, was achieved by first marking a piece of photographic film, attached to the specimen, with the X-ray beam at two locations of known X–Y co-ordinates. This was followed by marking the specimen though the film with a hole-punch, and subsequent parallel hole drilling (0.5 mm diameter) through the specimen thickness.

Crack shape results

The metallographic serial sectioning allowed measurement of the co-ordinates of the environment-assisted crack tip and the fatigue pre-crack tip in the strain-mapped volume, relative to the drilled holes, and hence three-dimensional determination of the crack shape. Small crack bridging ligaments (e.g. Fig. 2b) were observed in all the metallographic sections between the two positions. The positions of the initial fatigue pre-crack tip and the final environment-assisted crack tip are shown in Fig. 5 for (a) the Y–Z plane and (b) the X–Y plane. The strain-mapped volume within which the diffraction data were obtained is also marked. The crack mouth in this figure was defined as the position where the fatigue crack intersected the edge of the rectangular sample, and was therefore not the true

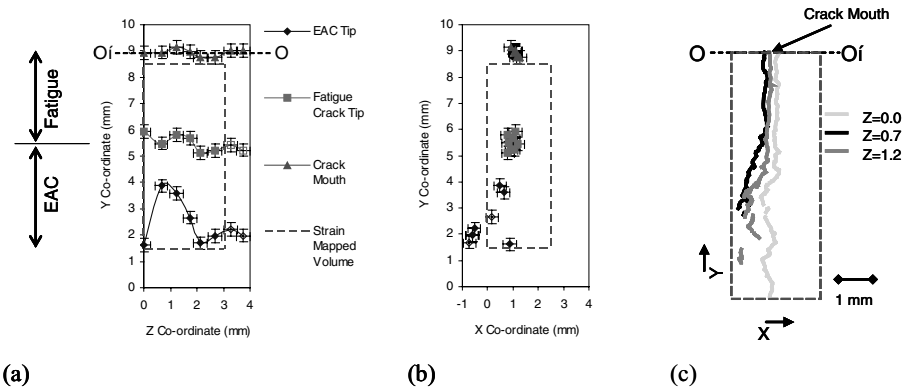

Fig. 5 Positions of crack tip, first crack bridge and crack mouth, determined by serial sectioning of the specimen. (a) projection in the Y–Z plane perpendicular to surface, (b) projection in X–Y plane parallel to the surface. (c) selected crack profiles in the X–Y plane. The approximate strain-mapped volume (defined by the mapped X–Y plane and diffraction gauge volume) is indicated. Open symbols represent points more than 3 mm from the surface. The directions of the X and Y coordinates, and the reference line O–O′ are indicated in Fig. 4.

crack mouth position in the original specimen. Its approximate position is marked by the line O–O′. The scatter in the observed position of the crack mouth Y co-ordinate (Fig. 5a) was consistent with the expected 0.25 mm error in position alignment, and this was also taken as the error in the positions of the fatigue and environment-assisted crack tips.

The fatigue crack was quite straight-fronted and flat, lying in the Y–Z plane. The environment-assisted crack, however, had an irregular front and had bifurcated (Fig. 5a). This is shown more clearly in Fig. 5c, in which the profile for the crack in the X–Y plane at the specimen surface ($Z = 0$) is compared with the profiles at distances of 0.7 and 1.2 mm. The environment-assisted crack tip had split into two branches within the strain-mapped volume. Close to the surface, the crack extended in the same plane as the fatigue pre-crack, and its tip was within the strain-mapped region. Below a distance of approximately 1 mm from the surface, the crack was inclined at approximately 25° to the fatigue crack, with a crack tip that was not fully within the mapped volume. Between these two branches, there was a substantial ligament of uncracked material. This is also apparent in Fig. 5a.

Synchrotron strain-mapping results

The elastic strains were first estimated by comparing the measured d_{hkl} with nominal spacing for the lattice parameter of pure iron ferrite and austenite, in the unloaded condition. This is an approximation because the unit cell parameters are affected by alloying. In the regions of the sample remote from the crack tip, i.e. in the wake of the fatigue crack, the calculated elastic strains in the austenite and ferrite were both calculated to be approximately -2200μ strain (± 400). Because the average elastic strain in this unloaded region was expected to be zero, a correction of 2200μ strain was applied to both phases at all loads. The corrected elastic strain was then converted to an approximate stress using a nominal elastic modulus of 200 GPa for both ferrite and austenite. This approximation was justified as the experimental noise, which resulted from the intergranular strains due to anisotropic elastic deformation, was a more significant source of error than the assumption of a common elastic modulus and strain correction for both ferrite and austenite.

The stress map obtained for austenite at an applied stress intensity factor of 60 MPa $m^{1/2}$ is shown in Fig. 6a. The stresses in the ferrite had a similar pattern to those in the austenite. It was not possible to clearly identify the crack in the stress map, and a composite image of all of the serial sections of the crack has been superposed onto the austenite stress map in Fig. 6b. The boundary between the fatigue and EAC components of the crack is marked. A crack tip stress concentration was not observed. Although the crack at the initial surface ($Z = 0$) lay within the mapped region (Fig. 5c), the bifurcated section of the crack below the surface had its tip outside of the strain-mapped volume. The mapped volume contained part of a significant crack bridging ligament.

Figure 6 shows that there was no significant variation in stress across the width of the stress map. The variation of stress, perpendicular to the crack plane, along the crack length was therefore described using the average stress over the width of the stress map. This was calculated for both ferrite and austenite, and is given in Fig. 7. This confirms there were similar raised stresses in both ferrite and austenite over the region between environment-assisted crack tip and the fatigue crack tip. This was the region containing the significant ligament between two branches of the bifurcated crack.

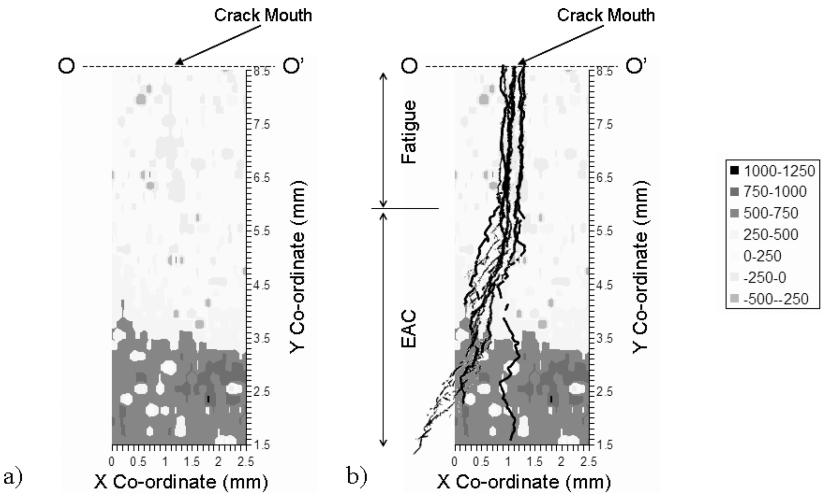

Fig. 6 (a) The variation of mode I stress (MPa) in the austenite and an applied stress intensity factor, K, of 60 MPa $m^{1/2}$. The crack profiles, determined by parallel serial sections are superposed in (b). The stresses were calculated from crystal lattice strains parallel to the X-coordinate direction with a nominal elasric modulus of 200 GPa, corrected by a constant strain of -2200μ strain to give zero average tensile stress remote from the crack tip.

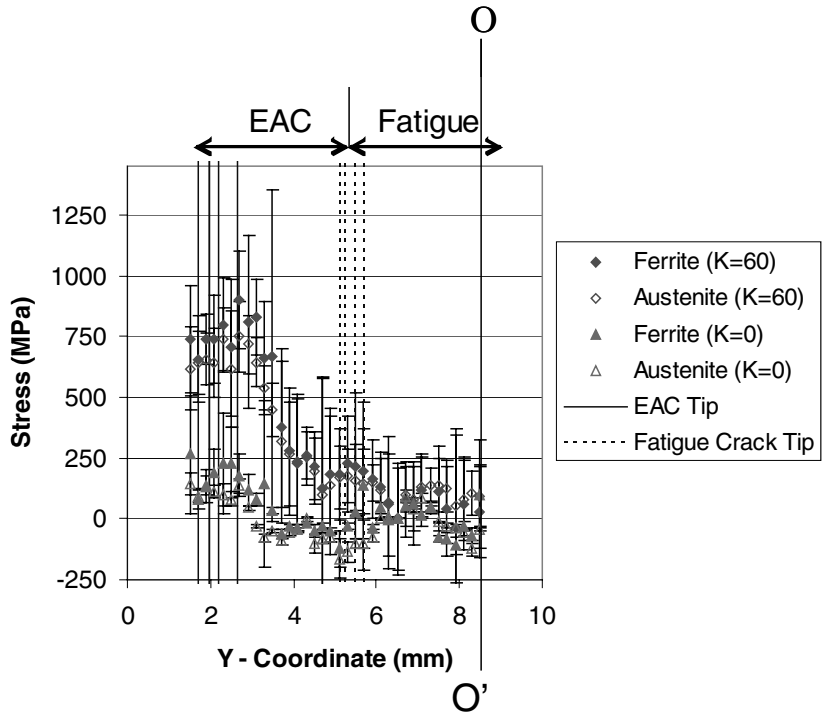

Fig. 7 Average mode I stress in ferrite and austenite across the width of the strain-mapped volume, as a function of position along the crack (Y-cordinate defined in Fig. 4). Data are given for the specimen in an unloaded ($K = 0$ MPa $m^{1/2}$) and loaded ($K = 60$ MPa $m^{1/2}$) condition. The positions of the environment-assisted crack tip and the fatigue pre-crack tip for all the metallographic sections through the gauge volume (Fig. 5) are marked.

DISCUSSION

When the crack was loaded, the stresses perpendicular to the crack were clearly raised in the zone between the environment-assisted crack tip and the fatigue crack tip. There is no significant stress in this zone when the crack is unloaded (Fig. 7). This can be understood as the effect of the bifurcated crack within in the strain-mapped region (Fig. 5).

The observation of mode I stresses between the environment-assisted crack tip and the fatigue crack tip implied that there were tractions in the crack wake which restricted the opening of the environment-assisted crack. This was in agreement with the observations of significant crack bridging ligaments (e.g. Fig. 5 and Fig. 2d) and the specimen compliance variation (Fig. 3). The crack wake tractions would shield the crack tip from the applied load, and increase the effective resistance to crack propagation. The magnitudes of the stresses over the length of the environment-assisted crack (Fig. 7) were consistent with those expected for the simple crack

bridging model for the observed *R*-curve behaviour (Fig. 1). The observation that the highest stresses were closest to the environmentally assisted crack tip (Fig. 7) was consistent with the increasing distance between the crack branches, and the resultant increased stiffness of the crack bridging ligament.

In principle, it would be possible to develop a more sophisticated calculation to more accurately evaluate the effect of the measured bridging stresses, using the weight function for the specimen geometry for example. However, the accuracy of the data does not currently warrant this. More detailed and extensive measurements using synchrotron diffraction could also be used to measure the elastic stress distribution around the crack tip, and thus measure more directly the shielding effect of crack bridging.

This experiment demonstrates the potential for high resolution synchrotron diffraction studies of elastic strains and hence the internal stress state in bulk specimens. This has a number of potential applications. For example, the internal stress state in a component can either assist or retard the nucleation and propagation of cracks. Furthermore, crack propagation usually leads to a stress re-distribution in components. The rate of crack growth and development of its path are affected by the stress state and processes such as branching of environment-assisted cracks and closure of fatigue cracks. Such processes may be studied, in situ, using high resolution synchrotron diffraction.

CONCLUSION

Synchrotron X-ray diffraction measurements can be used to characterize the elastic strains within bulk specimens of duplex stainless steel. The observations demonstrate that significant crack bridging stresses develop in the wake of a branched environment-assisted crack tip. Simple bridging models for the shielding contribution of the stress are in agreement with the observed *R*-curve behaviour.

Acknowledgements

The authors are grateful to Thomas Buslaps of the ESRF for his support during the experiment, and the ESRF for providing access to synchrotron X-rays through proposal number ME451.

REFERENCES

1 Francis, R., Byrne, G. and Warburton, G. R. (1997) Effects of cathodic protection on duplex stainless steels in seawater. *Corrosion* **53**, 234–240.
2 Owen, R. A., Preston, R. V., Withers, P. J., Shercliff, H. R. and Webster, P. J. (2003) Neutron and synchrotron measurements of residual strain in an aluminium alloy TIG weld. *Mater. Sci. Engng.* **A346**, 159–167.
3 Preuss, M., Withers, P. J., Maire, E. and Buffiere, J.-Y. (2002) SiC single fibre full-fragmentation during straining in a Ti-6Al-4V matrix studied by synchrotron X-rays. *Acta Mater.* **50**, 3175–3190.
4 Reimers, W., Broda, M., Brusch, G., Dantz, D., Liss, K. D., Pyzalla, A., Schmackers, T. and Tschentscher, T. (1998) Evaluation of residual stresses in the bulk of materials by high energy synchrotron diffraction. *J. Nondestruct. Eval.* **17**, 129–140.
5 Steuwer, A., Santisteban, J. R., Turski, M., Withers, P. J. and Buslaps, T. (2004) High-resolution strain mapping in bulk samples using full-profile analysis of energy-dispersive synchrotron X-ray diffraction data. *J. Appl. Crystallogr.* **37**, 883–889.
6 Marrow, T. J., Kim, S. and Oh, J.-T. (1999) The effect of microstructure on brittle fracture and stress corrosion cracking in duplex stainless steel. *Stainless Steels World 99*, The Hague, November 1999, KCI Publishing BV, pp. 721–727.
7 Kim, S. and Marrow, T. J. (1999) Application of electron backscattered diffraction to cleavage fracture in duplex stainless steel. *Scr. Mater.* **40**, 1395–1400.
8 Marrow, T. J., Humphreys, A. O. and Strangwood, M. (1997) The crack initiation toughness for brittle fracture of super duplex stainless steel. *Fatigue Fract. Engng Mater. Struct.* **20**, 1005–1014.
9 Mohammed, F. (2003) Stress corrosion cracking in duplex stainless steels. PhD thesis, UMIST, University of Manchester Institute of Science and Technology, UK.
10 ASTM Standard E 399-90 (Reapproved 1997) Standard test method for plane-strain fracture toughness of metallic materials. *American Society for Testing and Materials*, *Annual Book of ASTM Standards*, Vol. 03.01.
11 Novak, S. R. and Rolfe, S. T. (1969) Modified WOL specimen for K_{ISCC} environmental testing. *J. Mater.* **4**, 701–728.
12 Barinov, S. M. (1997) On crack-face bridging in a particulate ceramic-metal composite. *J. Mater. Sci. Lett.*, **16**, 1827–1829.